Biosensors and Bioelectronics 156 (2020) 112146

Contents lists available at ScienceDirect

Biosensors and Bioelectronics

journal homepage: http://www.elsevier.com/locate/bios

A three-dimensional DNA nanomachine with target recycling amplification technology and multiple electrochemiluminescence resonance energy transfer for sensitive microRNA-141 detection

Cun Wang [a,b], Min Chen [a], Qian Han [a,c], Jingling Wu [a], Xin Zhao [b], Yingzi Fu [a,*]

[a] Chongqing Engineering Laboratory of Nanomaterials & Sensor Technologies, School of Chemistry and Chemical Engineering, Southwest University, Chongqing, 400715, China

[b] Chongqing Collaborative Innovation Center for Functional Food, Chongqing University of Education, Chongqing, 400067, China

[c] Laboratory of Environment Change and Ecological Construction of Hebei Province, College of Resources and Environment Science, Hebei Normal University, Shijiazhuang, Hebei, 050024, China

ARTICLE INFO

Keywords:
Electrochemiluminescence
Multiple resonance energy transfer
Platinum nanoclusters
DNA nanomachine
Target recycling amplification technology
MicroRNA-141

ABSTRACT

An electrochemiluminescence (ECL) three-dimensional (3D) DNA nanomachine is developed for microRNA-141 (miRNA-141) detection by coupling Pb^{2+} dependent DNAzyme assisted target recycling amplification technology with multiple ECL resonance energy transfer (ECL-RET) system. Firstly, Pb^{2+} dependent DNAzyme is formed by three single strand DNA (ssDNA): A1, A2 and the target miRNA-141. In the presence of Pb^{2+}, the specific recognition site of the DNAzyme is cleaved and a large number of secondary targets (A3) are released. Secondly, the 3D DNA nanomachine consists of four ssDNA: H1, H2, H3 and the probe (two ends are labeled with alexa fluor (AF) and a nanocomposite (PtNCs@Ru(dcbpy)$_3^{2+}$) which is prepared by polyethyleneimine platinum nanoclusters and tris(4,4′-dicarboxylicacid-2,2′-bipyridyl) ruthenium(II) dichloride). Then, the 3D DNA nanomachine is assembled on the gold nanoparticles modified glassy carbon electrode. Afterwards, A3 is employed to hybridize with the probe, triggering the movement of the nanomachine and forming the multiple ECL-RET system. In this system, AF, serves as an effective energy transfer donor, which can transfer energy to PtNCs and Ru(dcbpy)$_3^{2+}$directly. Meanwhile, PtNCs, both as the acceptor and donor, can accept energy from AF and transfer it to Ru(dcbpy)$_3^{2+}$. As a result, The biosensor achieves enhanced ECL efficiency, which is 1.78 times that of the classic tris(2,2′-bipyridyl)ruthenium(II) dichloride (Ru(bpy)$_3^{2+}$) and exhibits good responses to miRNA-141 in the linear range from 10 aM to 100 nM with a detection limit of 3.3 aM. Also, the obtained biosensor can be employed to detect miRNA-141 in human serum samples, which will be of great significance in bioanalysis.

1. Introduction

MicroRNA-141 (miRNA-141), an endogenous, short and single-stranded noncoding RNA with 22 nucleotides, participates in cellular proliferation, differentiation and apoptosis process (Croce et al., 2005). Normally, the abnormal expression (down or up-regulation) of miRNA-141 correlates with various types of human cancers, including cancers of breast, ovarian, colorectal, pancreatic and others (Lee et al., 2015; Liu et al., 2017b; Shi et al., 2018). Several approaches have been applied to detect miRNA-141, such as fluorescence, electrochemistry, photoelectrochemistry and electrochemiluminescence (Li et al., 2019; Lu et al., 2018; Zhang et al., 2018a; Zhang et al., 2019). However, some disadvantages of complex operation, high cost of the production and low sensitivity hinder the effective detection. Hence, to develop a simple, reliable, relatively economical and sensitive method for the analysis of miRNA-141 is of great significance.

Electrochemiluminescence resonance energy transfer (ECL-RET) is a widely used spectroscopy method occurring between matched energy donor/acceptor pair, which is based on the non-radiative energy transfer mechanism (Huo et al., 2018; Lu et al., 2018;; Sha et al., 2019). Owing to the combination of ECL and RET, the ECL-RET system has been demonstrated to be one of the most practical and useful approach in bioanalysis (Chen et al., 2018; Zhang et al., 2017a). Despite the luminous efficiency of the classic ECL-RET system has been improved, it is prone to cause energy loss and efficiency reduction, owing to the long distance between a single energy donor and a single acceptor (Li et al.,

* Corresponding author.
E-mail address: fyzc@swu.edu.cn (Y. Fu).

https://doi.org/10.1016/j.bios.2020.112146
Received 3 November 2019; Received in revised form 21 February 2020; Accepted 9 March 2020
Available online 10 March 2020

2017; Chen et al., 2018). Therefore, it is still necessary to develop an efficient ECL-RET system. Nanocomposites containing both energy donor and acceptor has been used in this purpose (Li et al., 2017). However, the application of multiple ECL-RET in biosensor is rarely.

In recent years, diverse DNA molecular machines including the DNA nanogear, DNA walking machine, DNA tweezer and DNA nanomachine have been creatively used for detection of miRNA and disease biomarker (Lv et al., 2018, 2020; Zhang et al., 2017a,b; Zhuang et al., 2014). In particular, the new next generation of 3D DNA nanomachine for miRNA detection has been proposed (Zhang et al., 2018b). Due to the organized and high local concentration of nippers, it significantly enhances the movement efficiency and simplifies the complex operating procedures of the traditional 3D DNA nanomachine (Feng et al., 2018a,b). Improving the sensitivity has been always the research direction of 3D DNA nanomachine based biosensors. Therefore, a variety of amplification strategies are emerged such as enzyme-assisted DNAzymes and metal ion-dependent DNAzymes (Xu et al., 2016; Kim et al., 2007). Among them, Pb^{2+} dependent DNAzyme is a sequence-specific nuclease with the advantages of high catalytic activity, simple operation, low production cost, and reusable. It can catalyze a series of biological and biochemical reactions, and overcome the shortcomings of conventional enzymes and enzyme-assisted DNAzymes (Kim et al., 2007). And in the presence of Pb^{2+}, the specific recognition site of the DNAzyme is cleaved, leading to the release of the target miRNA for the next cycle. (Kim et al., 2007; Xu et al., 2018).

Herein, we report a 3D DNA nanomachine with multiple ECL-RET and Pb^{2+} dependent DNAzyme assisted target recycling amplification technology for microRNA-141 detection. In the first, a nanocomposite (PtNCs@Ru(dcbpy)$_3^{2+}$) composed of polyethyleneimine platinum nanoclusters (PtNCs) and tris(4,4′-dicarboxylicacid-2,2′-bipyridyl) ruthenium(II) dichloride (Ru(dcbpy)$_3^{2+}$) is synthesized. Since the energy donor (PtNCs)/acceptor (Ru(dcbpy)$_3^{2+}$) pair exist in the same nanostructure, which shortens the electron-transfer path, reduces the energy loss and enhances the RET efficiency. Secondly, multiple energy transfer donor/acceptor pairs are introduced into the ECL-RET system to construct the multiple ECL-RET. Thirdly, with the help of Pb^{2+} dependent DNAzyme assisted target recycling amplification technology, a 3D DNA nanomachine based biosensor is constructed to achieve simple, efficient and sensitive detection of miRNA-141, which can be extended as a general sensitive platform for detecting various RNA cancer biomarkers.

2. Experimental section

2.1. Synthesis of the PtNCs and PtNCs@Ru(dcbpy)$_3^{2+}$

The polyethyleneimine platinum nanoclusters (PtNCs) were synthesized by one-step hydrothermal method (Xu et al., 2017). Firstly, 0.1668 g polyethyleneimine (PEI) was added into 20 mL 2.5 mM $H_2PtCl_6 \cdot 6H_2O$ solution. Here PEI was used as a stabilizer. After the solution was stirred at room temperature for 2 h, 1.8 mg ascorbic acid (AA) was added to the above solution. Then 1.0 M HCl was used to adjust the pH to 5.0. The PtNCs with plenty of PEI were obtained after the hydrothermal reaction at 90 °C for 1 h. Finally, the synthesized PtNCs were purified by a 2000 Da dialysis membrane for 48 h, and stored at 4 °C.

The PtNCs@Ru(dcbpy)$_3^{2+}$ was obtained as follows. Briefly, the carboxyl groups of Ru(dcbpy)$_3^{2+}$ were activated using EDC/NHS (4:1) solution for 2 h at 4 °C. Then 0.1 mL of 0.05 M Ru(dcbpy)$_3^{2+}$ solution was added into the 30 mL PtNCs solution. Finally, the mixture solution was continuously stirred at room temperature for 24 h to synthesis the PtNCs@Ru(dcbpy)$_3^{2+}$ nanocomposite via amide covalent bond. As a control experiment, PEI platinum nanoparticles (PtNPs) were prepared in accordance with the reported methods (Liu et al., 2017) and PtNPs@Ru(dcbpy)$_3^{2+}$ nanocomposites were synthesized through the similar process.

2.2. Preparation of the Pb^{2+} dependent DNAzyme and the 3D DNA nanomachine

The Pb^{2+} dependent DNAzyme was prepared according the reported method (Kim et al., 2007). First, gold nanoparticles (AuNPs) were synthesized (Frens et al., 1973). Second, 1 mL of 5 mg mL^{-1} amino-modified magnetic polystyrene microspheres (NH_2-PSC) solution was added to the 4 mL AuNPs solution and stirred for 2 h at 4 °C. The mixture was centrifuged, washed and redispersed in 3 mL PBS (0.1 M, pH 7.0) to obtain PSC@AuNPs. Then 50 μL PSC@AuNPs were blended with 50 μL 2 μM A1 overnight at 4 °C. After magnetic separation of the unbonded A1, the obtained A1-PSC@AuNPs were incubated with 50 μL 2 μM A2 and 50 μL varying concentrations of miRNA-141 for 90 min at 37 °C to form the DNAzyme. Subsequently, the specific recognition site of the DNAzyme was cleaved by 10 μM Pb^{2+}. Through the magnetic separation, the gained solution with a large number of secondary target (A3) was stored at 4 °C for further use.

The 3D DNA nanomachine was synthesized as follows. The carboxyl groups of alexa fluor (AF, 250 μL, 0.5 mg L^{-1}) were activated using the EDC/NHS (4:1) solution for 2 h at 4 °C, followed by the addition of amino-modified probe for 2 h to obtain the AF-probe (Zhang et al., 2018b). Under continuous stirring, the thiol modified AF-probe connected with PtNCs@Ru(dcbpy)$_3^{2+}$ via Pt–S bond. Subsequently, the AF-probe-PtNCs@Ru(dcbpy)$_3^{2+}$ was centrifuged and washed thoroughly. After that, the equimolar amount of AF-probe-PtNCs@Ru(dcbpy)$_3^{2+}$, H1, H2 and a small amount of capture DNA strand H3 were mixed together and heated to 95 °C for 2 min. Finally, the mixture was placed on ice for 3 min to synthesize the 3D DNA nanomachine. The 3D DNA nanomachines with different nanomaterial functionalized probes, such as PtNCs@Ru(dcbpy)$_3^{2+}$, AF-PtNCs or AF-PtNPs@Ru(dcbpy)$_3^{2+}$ labeled probes were synthesized as the control experiment.

2.3. Assembly of the sensing electrode

Each bare glassy carbon electrode (GCE, diameter 4.0 mm) was polished and washed with ethanol and water thoroughly. Then AuNPs modified GCE (AuNPs/GCE) was obtained by immersing the GCE into 1% $HAuCl_4$ solution and electrodepositing under −0.2 V for 30 s. Afterwards, 10 μL of 3D DNA nanomachine was dropped on AuNPs/GCE and incubated overnight at 4 °C to obtain the 3D DNA nanomachine/AuNPs/GCE. Further, 10 μL of A3 was dropped and incubated for 90 min to open the probes of the 3D DNA nanomachine, resulting in changes in biosensor signals. Finally, the biosensor was incubated with DNA strand S1 at 37 °C for 90 min to achieve the regeneration by chain replacement method.

3. Results and discussion

3.1. Amplified miRNA-141 detection principle in multiple ECL-RET system

Our approach for miRNA-141 detection is illustrated in Scheme 1. As shown in scheme 1A, the 3D DNA nanomachine is prepared by using four single strands DNA (ssDNA): one probe (two ends are labeled with AF and PtNCs@Ru(dcbpy)$_3^{2+}$ respectively), two assisted ssDNA: H1 and H2, and one capture DNA strand (H3). After a simple annealing process, probe, H1, H2 and H3 are self-assembled together to form a 3D DNA nanomachine. As the foot of the 3D DNA nanomachine, H3 can fix the 3D DNA nanomachine onto the surface of gold nanoparticles (AuNPs) modified glassy carbon electrode. From scheme 1B, the Pb^{2+} dependent DNAzyme is formed by one target miRNA-141 and two helper ssDNA (A1 and A2). The specific recognition site of DNAzyme can be cleaved by Pb^{2+}, releasing the target miRNA-141 and A2, and generating the secondary target DNA (A3). The target miRNA-141 and A2 hybridize with A1 again to initiate the next recycling, and then generate more A3. As can be seen from scheme 1C, A3 can hybrid with the 3D DNA

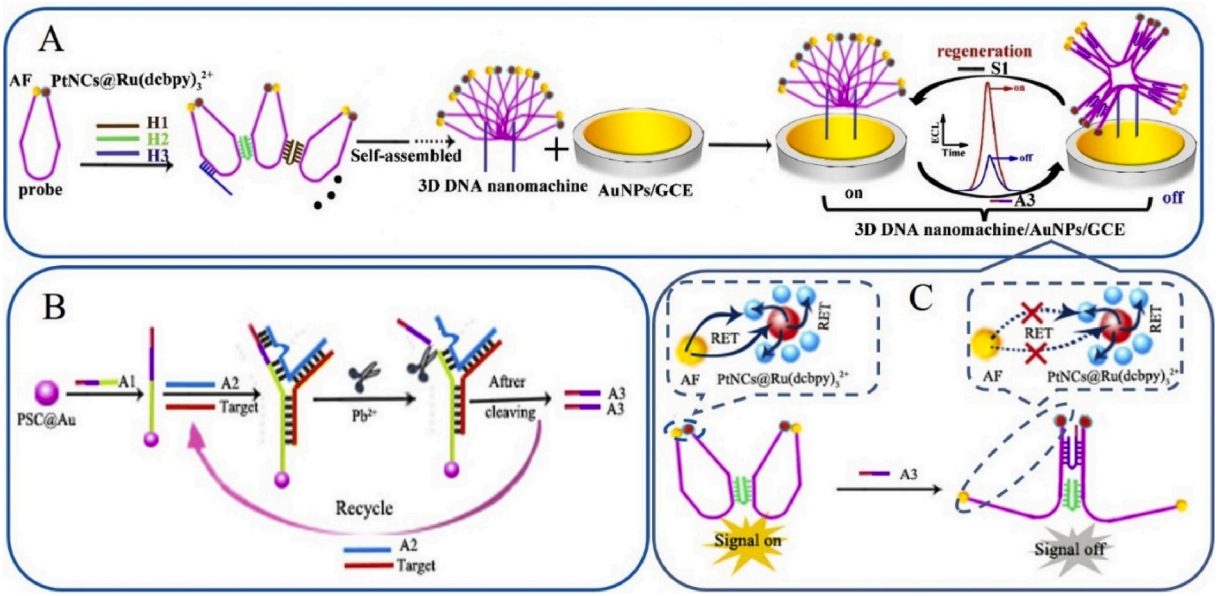

Scheme 1. Schematic illustration of (A) the 3D DNA nanomachine assembled biosensor, (B) target recycling amplification technology and (C) the multiple ECL-RET.

nanomachine probe strands and make the probes in the "open" state, the distance between AF and PtNCs@Ru(dcbpy)$_3^{2+}$ is long, resulting in a low ECL signal. In the absence of A3, the probes are in the "close" state to form a multiple ECL-RET. In this system, AF is an effective energy transfer donor to transfer energy directly to PtNCs and Ru(dcbpy)$_3^{2+}$. And as a bridge in energy transfer, PtNCs can receive (from AF) and transfer (to Ru(dcbpy)$_3^{2+}$) energy. That is to say, PtNCs play dual roles, not only as a donor, but also as an acceptor. So the ECL intensity can be greatly enhanced through the multiple ECL-RET. Finally, the regeneration of the biosensor can be achieved by a simple chain replacement method, which reduces the manufacturing cost to a certain extent.

3.2. Characterization of 3D DNA nanomachine, PtNCs and PtNCs@Ru (dcbpy)$_3^{2+}$

Polyacrylamide gel electrophoresis (PAGE) was employed to verify the feasibility of the Pb^{2+} dependent DNAzyme and the 3D DNA nanomachine. As shown in Fig. 1A, the distinct bands in lane 1–3 correspond to the ssDNA of A1, A2 and miRNA-141, respectively. After incubation the above three ssDNA at 37 °C for 90 min, a single and bright band is shown in lane 4, suggesting the successful assembly of the Pb^{2+} dependent DNAzyme. Meanwhile, as seen from Fig. 1B, the clear and bright bands in lane 2–5 represent the ssDNA of probe, H3, H2 and H1. Through the one-step annealing reaction of probe, H1, H2 and H3, a reduced electrophoretic mobility is exhibited on the band of lane 1, hinting the successful formation of the 3D DNA nanomachine.

The morphologies of PtNCs and PtNCs@Ru(dcbpy)$_3^{2+}$ were characterized by transmission electron microscopy (TEM) and dynamic light scattering (DLS). PtNCs (Fig. S1) and PtNCs@Ru(dcbpy)$_3^{2+}$ (Fig. S2) exhibit approximately spherical structures with the hydrodynamic diameters of 1.7 ± 0.6 nm and 2.4 ± 0.5 nm, respectively. And the elemental composition of PtNCs@Ru(dcbpy)$_3^{2+}$ was evaluated by X-ray photoelectron spectroscopy (XPS). The characteristic peaks of elements for Ru3P, Pt4f, C1s, N1s O1s, and Cl2p are observed obviously (Fig. S3). Besides, the elemental distribution image of PtNCs@Ru(dcbpy)$_3^{2+}$ was also obtained by energy dispersive X-ray (EDX) spectrum (Fig. S4). The elements of C, N, O, Si, Cl, Pt and Ru are clearly observed from the EDX mappings. These results indicate that the nanocomposite of PtNCs@Ru (dcbpy)$_3^{2+}$ has been successfully synthesized.

As a key step for the biosensor, the 3D DNA nanomachine was further characterized by atomic force microscope (AFM), transmission electron microscopy (TEM) and DLS. From Fig. 2A and B, 3D DNA nanomachines with uniform structures are displayed in AFM images. And they also appear as near-spherical structures (Fig. 2C), the average hydrodynamic diameter of the 3D DNA nanomachines is 21.0 ± 10.0 nm (Fig. 2D). The acquired AFM results of 3D DNA nanomachine are consistent with the

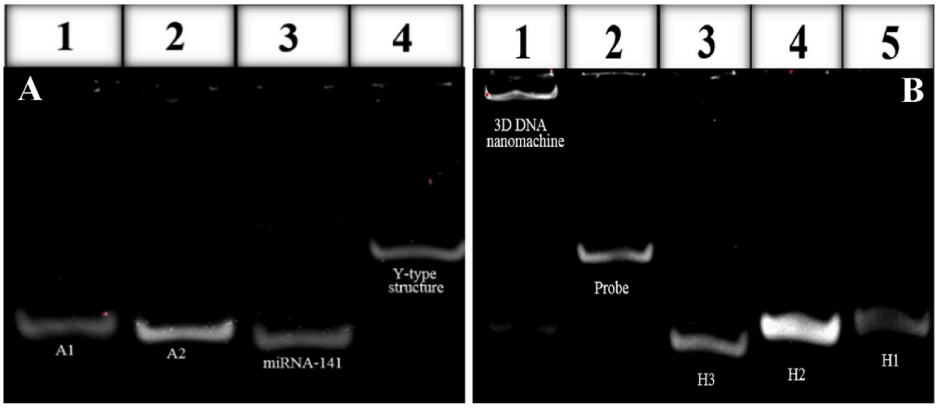

Fig. 1. The PAGE characterization: (A) lane 1, A1; lane 2, A2; lane 3, miRNA-141; lane 4, the Pb^{2+} dependent DNAzyme; (B) lane 1, 3D DNA nanomachine; lane 2, probe; lane 3, H3; lane 4, H2; lane 5, H1 (All DNA concentrations are 1 μM).

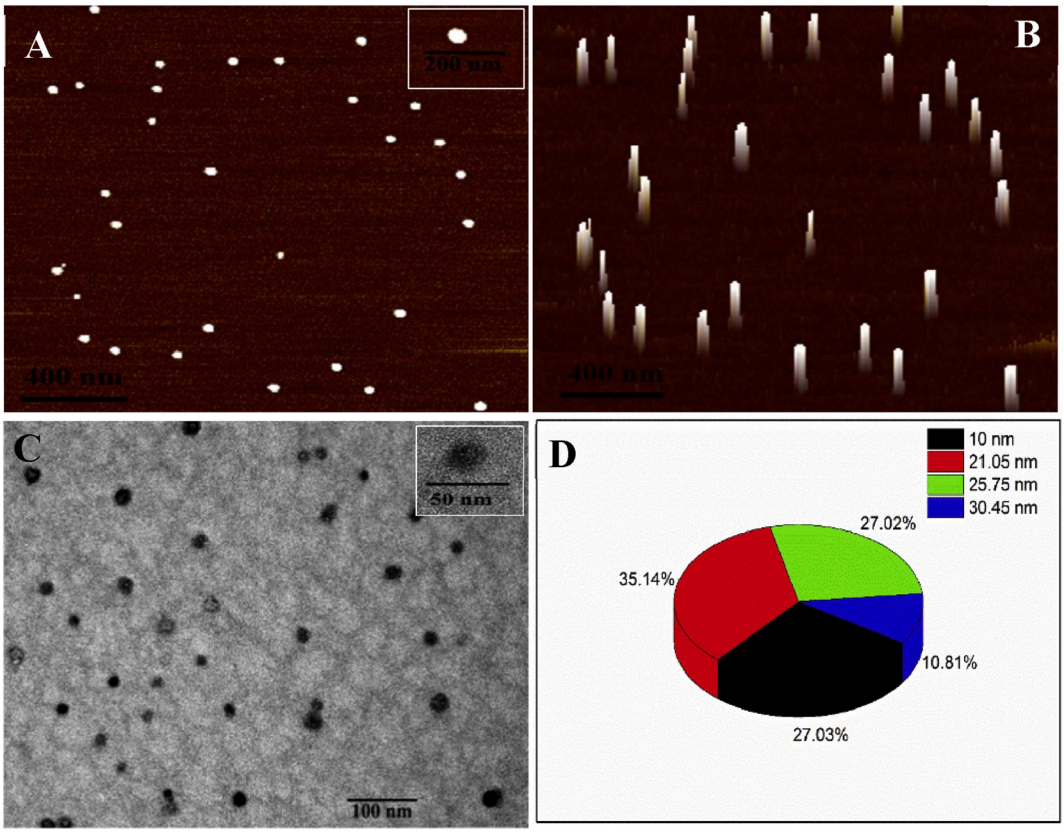

Fig. 2. (A, B) AFM, (C) TEM and (D) DLS characterization of 3D DNA nanomachines.

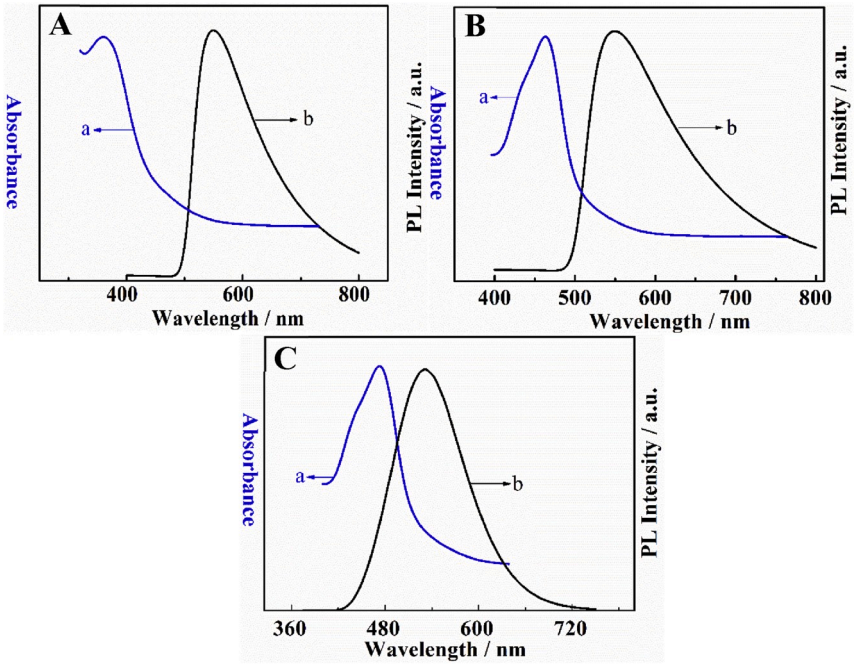

Fig. 3. (A) (a) The UV–vis absorption spectrum of PtNCs and (b) the PL spectrum of AF; (B) (a) The UV–vis absorption spectrum of $Ru(dcbpy)_3^{2+}$ and (b) the PL spectrum of AF; (C) (a) The UV–vis absorption spectrum of $Ru(dcbpy)_3^{2+}$ and (b) the PL spectrum of PtNCs.

TEM results and literature (Zhang et al., 2018b).

3.3. Feasibility demonstration of the multiple ECL-RET system

To confirm the multiple RET, the photoluminescence (PL) emission spectra of the donor (AF and PtNCs) and the UV–vis absorption spectra of the acceptor (PtNCs and $Ru(dcbpy)_3^{2+}$) were investigated. First, it is found that the PL emission spectrum of the AF overlaps with both the UV–vis absorption spectra of PtNCs (Fig. 3A) and $Ru(dcbpy)_3^{2+}$ (Fig. 3B), indicating that RET can be generated not only between AF and PtNCs but

also between AF and $Ru(dcbpy)_3^{2+}$.Then, the PL emission spectrum of the PtNCs overlaps with the UV–vis absorption spectrum of $Ru(dcbpy)_3^{2+}$ (Fig. 3C), displaying the presence of RET between PtNCs and Ru $(dcbpy)_3^{2+}$. Here we can see that PtNCs play double roles of the donor and the acceptor in the multiple ECL-RET system.

According to the control experiment (Fig. S5), the strongest ECL intensity is obtained from the proposed biosensor (Fig. S5D), revealing that the final efficiency of the ECL-RET system can be significantly enhanced by the multiple RET effect. The reason lies in multiple energy donor/acceptor pairs existed in the same nanostructure, which shorten the electron-transfer path, reduce the energy loss and enhance the RET efficiency (Li et al., 2017; Chen et al., 2018). And the calculated ECL efficiency of $Ru(dcbpy)_3^{2+}$ in our work is 1.78 times that of the classic Ru $(bpy)_3^{2+}$ (Supplementary Material, Eq. (1)).

3.4. Analytical performance of the proposed biosensor

Electrode modification procedures were characterized by cyclic voltammetry (CV) and electrochemical impedance spectroscopy (EIS) (Fig. S6). Under optimized experimental conditions (Fig. S7), the analytical performance of the proposed biosensor was detected by incubation with various concentrations of miRNA-141. It can be clearly seen in Fig. 4, the ECL intensity obviously decrease with the increasing concentration of target miRNA-141 from 10 aM to 100 nM. The linear regression equation is found to be $I = 797.03–672.88 \lg c$ ($R^2 = 0.971$), and the limit of detection is estimated to be 3.3 aM (S/N = 3). Compared with the previous methods, our biosensor shows an improved sensitivity and a broader linear range (Table S1).

3.5. Selectivity, stability and regenerability

To evaluate the selectivity of the proposed biosensor, some possible interferences such as miRNA-182–5P, miRNA-21, miRNA-155 and the specific protein thrombin (TB) were assessed. As evidenced by Fig. 5A, the ECL intensities similar to the blank sample appear with the addition of the interfering agents (1 nM), whereas a significant reduction ECL intensity is obtained when the target miRNA-141 is added even at a low concentration (1 pM) to the proposed biosensor. And the ECL intensity of the mixture (Mix: 1 pM target miRNA-141 and 1 nM interfering agents) and the 1 pM miRNA-141 is almost the same. These results suggest a good selectivity of the proposed biosensor for miRNA-141 determination. Besides, the stability of the biosensor is also examined. From Fig. 5B, no obvious change is observed in ECL intensity after 24 cycles of consecutive measurements of miRNA-141 (1 nM). The relative standard deviations (RSD) is 1.9%. Meanwhile, after 10 and 20 days of storage, the ECL intensities of this biosensor reduced by 8.8% and 22.7%, respectively. All above results indicate the good stability of the proposed biosensor.

Regeneration was also studied. As depicted in Fig. 5C, the biosensor is regenerated over three cycles for the analysis of miRNA-141 (100 fM), showing a certain regenerative capacity.

3.6. The application of the biosensor

To assess the applicability of the designed biosensor for real samples, healthy human serum samples (from the Ninth People's Hospital of Chongqing, China) were selected. Prior to testing, each sample was centrifuged and obtained the supernatant. Then, 50-fold diluted serum samples (by 0.1 M PBS, pH 7.0) with different concentrations of miRNA-141 (100 fM, 1 nM and 100 nM) were measured by standard addition method. As shown in Table S2, the spike recoveries ranged from 98.7% to 105.0% with RSD less than 2.8% (n = 6), which is acceptable for quantitative assays performed in real samples.

4. Conclusions

In summary, we have demonstrated a sensitive and selective miRNA-141 detection can be achieved by a 3D DNA nanomachine binding the Pb^{2+} dependent DNAzyme assisted target recycling amplification technology and multiple ECL-RET. Compared with the conventional ECL-RET system, our 3D DNA nanomachine based biosensor presents two advantages to significantly improve the ECL efficiency and sensitivity. One is due to the existence of multiple energy donor/acceptor pairs in the same nanostructure, resulting in a shorter electron-transfer path, less energy loss and higher RET efficiency. And the ECL efficiency is 1.78 times higher than the classic $Ru(bpy)_3^{2+}$. The other is with the help of the Pb^{2+} dependent DNAzyme assisted target recycling amplification technology, the proposed biosensor receives a higher sensitivity. Moreover, the proposed biosensor possesses high selectivity and can be applied to detect miRNA-141 in diluted human serum samples, which can be offered new opportunities for the development of convenient signal amplification strategies for detecting various RNA targets and early disease diagnosis.

Declaration of competing interest

The authors declare that they have no known competing financial interests or personal relationships that could have appeared to influence the work reported in this paper.

CRediT authorship contribution statement

Cun Wang: Investigation, Writing - original draft, Writing - review & editing. **Min Chen:** Conceptualization. **Qian Han:** Validation. **Jingling Wu:** Data curation. **Xin Zhao:** Software. **Yingzi Fu:** Funding acquisition, Project administration.

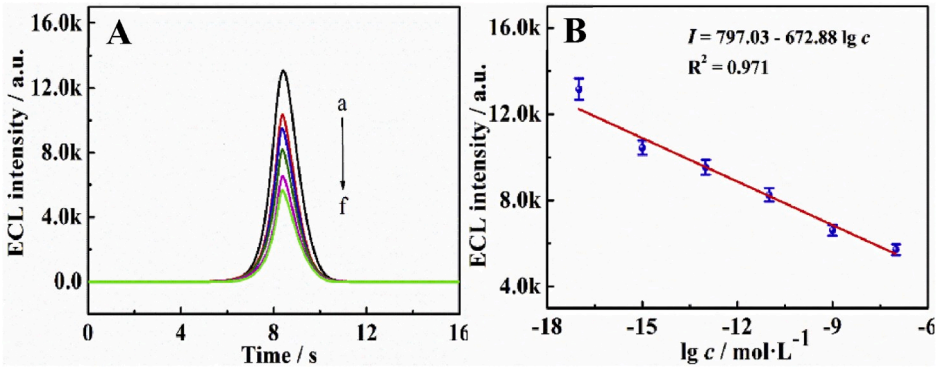

Fig. 4. (A) The ECL responses of the proposed biosensor for different concentrations of miRNA-141: (a) 10 aM, (b) 1 fM (c) 100 fM (d) 10 pM (e) 1 nM (f) 100 nM. (B) The calibration plot of ECL intensity vs the logarithm concentration of miRNA-141.

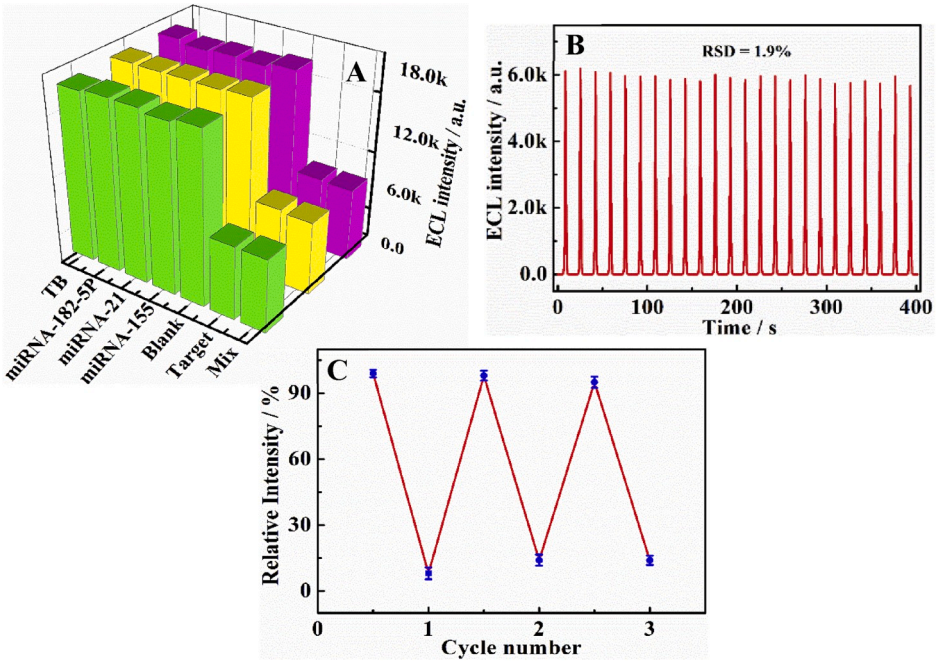

Fig. 5. (A) Selectivity of the proposed biosensor: blank sample, 1 nM interfering substances, including TB, miRNA-182–5P, miRNA-21 and miRNA-155, 1 pM target microRNA-141 and the Mix (1·pM microRNA-141 and 1 nM interfering substances). (B) The stability of the proposed biosensor (1 nM microRNA-141). (C) The biosensor response for miRNA-141 detection over three cycles.

Acknowledgment

This work is supported by the National Natural Science Foundation of China (No. 21272188) and the Science and Technology Research Project of Chongqing Municipal Education Commission (KJQN201901604).

Appendix A. Supplementary data

Supplementary data to this article can be found online at https://doi.org/10.1016/j.bios.2020.112146.

References

Chen, M.M., Wang, Y., Cheng, S.B., Wen, W., Zhang, X.H., Wang, S.F., Huang, W.H., 2018. Anal. Chem. 90, 5075–5081.
Croce, C.M., Calin, G.A., 2005. Cell 122, 6–7.
Feng, C., Wang, Z.H., Chen, T.S., Chen, X.X., Mao, D.S., Zhao, J., Li, G.X., 2018a. Anal. Chem. 90, 4932–4932.
Feng, C., Wang, Z.H., Chen, T.S., Chen, X.X., Mao, D.S., Zhao, J., Li, G.X., 2018b. Anal. Chem. 90, 2810–2815.
Frens, G., 1973. Nature 241, 20–22.
Huo, X.L., Zhang, N., Yang, H., Xu, J.J., Chen, H.Y., 2018. Anal. Chem. 90, 13723–13728.
Kim, H.K.Y., Liu, J.W., Li, J., Nagraj, N.D.N., Li, M.X., Pavot, C.M.B., Lu, Y., 2007. J. Am. Chem. Soc. 129, 6896–6902.
Lee, H., Srinivas, R.L., Gupta, A., Doyle, P.S., 2015. Angew. Chem. Int. Ed. 54, 2477–2481.
Li, Z.Y., Lin, Z.F., Wu, X.Y., Chen, H.T., Chai, Y.Q., Yuan, R., 2017. Anal. Chem. 89, 6029–6035.
Li, C.L., Li, H.K., Ge, J.J., Jie, G.F., 2019. Chem. Commun. 55, 3919–3922.
Liu, C., Liu, R.F., Zhang, D.X., Deng, Q., Liu, B.G., Chao, H.P., Rycaj, K., Takata, Y., Lin, K., Lu, Y., Zhong, Y., Krolewski, J., Shen, J.J., Tang, D.G., 2017a. Nat. Commun. 8, 14270–14283.
Liu, J.L., Tang, Z.L., Zhuo, Y., Chai, Y.Q., Yuan, R., 2017b. Anal. Chem. 89, 9108–9115.
Lu, H.J., Pan, J.B., Wang, Y.Z., Ji, S.Y., Zhao, W., Luo, X.L., Xu, J.J., Chen, H.Y., 2018. Anal. Chem. 90, 10434–10441.
Lv, S.Z., Zhang, K.Y., Zhu, L., Tang, D.P., 2020. Anal. Chem. 92, 1470–1476.
Lv, S.Z., Zhang, K.Y., Zeng, Y.Y., Tang, D.P., 2018. Anal. Chem. 90, 7086–7093.
Shi, L., Lei, J., Zhang, B., Li, B.X., Yang, C.Y.J., Jin, Y., 2018. ACS Appl. Mater. Interfaces 10, 12526–12533.
Sha, H.F., Zhang, Y., Wang, Y.F., Ke, H., Xiong, X., 2019. Biosens. Bioelectron. 124–125, 59–65.
Xu, M.D., Gao, Z.Q., Wei, Q.H., Chen, G.N., Tang, D.P., 2016. Biosens. Bioelectron. 79, 411–415.
Xu, N., Li, H.W., Wu, Y.Q., 2017. Anal. Chim. Acta 958, 51–58.
Xu, J.M., Zhang, Y., Li, L., Kong, Q.K., Zhang, L.N., Ge, S.G., Yu, J.H., 2018. ACS Appl. Mater. Interfaces 10, 3431–3440.
Zhang, P., Li, Z.Y., Wang, H.J., Zhuo, Y., Yuan, R., Chai, Y.Q., 2017a. Nanoscale 9, 2310–2316.
Zhang, P., Jiang, J., Yuan, R., Zhuo, Y., Chai, Y.Q., 2018b. J. Am. Chem. Soc. 140, 9361–9364.
Zhang, C.L., Li, D., Li, D.W., Wen, K., Yang, X.D., Zhu, Y., 2019. Analyst 144, 3817–3825.
Zhang, P., Lin, Z.F., Zhuo, Y., Yuan, R., Chai, Y.Q., 2017b. Anal. Chem. 89, 1338–1345.
Zhang, N., Shi, X.M., Guo, H.Q., Zhao, X.Z., Zhao, W.W., Xu, J.J., Chen, H.Y., 2018a. Anal. Chem. 90, 11892–11898.
Zhuang, J.Y., Lai, W.Q., Chen, G.N., Tang, D.P., 2014. Chem. Commun. 50, 2935–2938.